Evaluation of Residual Stresses in the Bulk of Materials by High Energy Synchrotron Diffraction

W. Reimers,[1] M. Broda,[1] G. Brusch,[1] D. Dantz,[1] K.-D. Liss,[2] A. Pyzalla,[1] T. Schmackers,[1] and T. Tschentscher[2]

High energy synchrotron diffraction is introduced as a new method for residual stress analysis in the bulk of materials. It is shown that energy dispersive measurements are sufficiently precise so that strains as small 10^{-4} can be determined reliably. Due to the high intensity and the high parallelism of the high energy synchrotron radiation the sample gauge volume can be reduced to approximately 50 μm $\times$ 1 mm $\times$ 1 mm compared to gauge volume of one mm³ up to several mm³ achievable by neutron diffraction. The benefits of the high penetration depth and the small gauge volume are demonstrated by the results of stress studies performed on a fiber reinforced ceramic, a functional gradient material and a metal–ceramic compound. Furthermore, it is shown that in case of a cold extruded metal specimen the energy dispersive measurement technique yields simultaneous information about texture and residual stresses and thus allows a detailed investigation of elastic and plastic deformation gradients.

KEY WORDS: Residual stress; high energy synchrotron diffraction; energy dispersive diffraction.

1. INTRODUCTION

Diffraction methods are widely used for the non-destructive evaluation of residual stresses in crystalline materials. Their basis in case of angle dispersive diffraction is the precise determination of the Bragg angle 2θ, whereas in the case of energy dispersive diffraction it is the precise determination of the energy of the Bragg reflection. From the shift of the diffraction profile the interplanar lattice distance and the corresponding strain can be evaluated. Applying Hooke's law yields the residual stresses.

High energy synchrotron diffraction, which is now available at modern synchrotron sources due to its high intensity, its high parallelism and its energy dispersive characteristic is a promising new method for residual stress analysis. The high intensity of the synchrotron beam gives access to penetration depths far beyond those of a few microns achievable by characteristic X-ray radiation. Beyond these few microns, information depths up to approximately 100 μm below the sample surface have been realized in the reflection mode by energy dispersive arrangements[1-3] using high energy X-ray laboratory sources resp. synchrotron radiation. Larger penetration depths up to some cm, thus allowing the analysis of bulk residual stresses, can be achieved by neutron diffraction.[4,5] Approximately similar penetration depths can be realized in the transmission mode by high energy X-ray diffraction in a laboratory.[3,6,7]

However, the comparatively poor intensity of the neutron beam as well as of laboratory X-ray sources requires a minimum sample gauge volume in the magnitude of one up to several mm³. Here, the use of a modern high energy synchrotron source like the ESRF in Grenoble, is much more favorable. Due to the high photon flux at very high energy synchrotron radiation, e.g., at

[1] Hahn-Meitner-Institut, Glienicker Strasse 100, D-14109 Berlin, Germany.
[2] European Synchrotron Radiation Facility ESRF, B.P. 220, F-38043 Grenoble Cedex, France.

the beamline ID 15 at the ESRF Grenoble, a reduction of the gauge volume into the 50 μm × 1 mm × 1 mm region is possible. Furthermore, the high parallelism of the synchrotron radiation guarantees the precise definition of the gauge volume as realized by diaphragm slit systems. Thus, high energy synchrotron diffraction due to the combinations of high intensity and high parallelism of the radiation, allows strain/stress investigations with high local resolution in the bulk of materials, enabling detailed analyses of stress gradients as they occur, for example, near interfaces.

Furthermore, due to its energy dispersive characteristic, residual stress analysis by high energy synchrotron diffraction, compared to residual analysis by monochromatic synchrotron diffraction,[8-11] offers the possibility of a simultaneous registration of several Bragg reflections, so yielding information about the residual stresses as well as about the eventual presence of texture at the same time.

Within this paper, some examples are presented in order to demonstrate the capability of high energy synchrotron diffraction in the field of residual stress analysis. First, an experiment is described which proves the possibilities of the method and the reliability of the obtained data. Then examples for the investigation of a fiber reinforced and a metal–ceramic gradient (FGM) composite are given, where the available local resolution is important for the interpretation of the results. Experiments concerning a ceramic metal layer compound reveal that even in an interface layer with a thickness of only 100 μm data could be obtained, which was not possible by any other nondestructive method before. Finally, investigations of a cold forward extruded sample are presented, where stress and texture gradients could be analyzed simultaneously.

2. BASIC PRINCIPLES OF ENERGY DISPERSIVE SYNCHROTRON DIFFRACTION FOR RESIDUAL STRESS ANALYSIS

In energy dispersive diffractometry, energy spectra are recorded at a fixed scattering angle 2θ. So a multitude of reflections from a polycrystalline sample at different energy values is analyzed simultaneously. The energy of the reflections represents the lattice spacing including the strain. A sufficient counting statistic and least square fitting of the reflection profile using a Gaussian curve enables the determination of the profile position so precisely that strains as low as 10^{-4} can be determined reliably.[12]
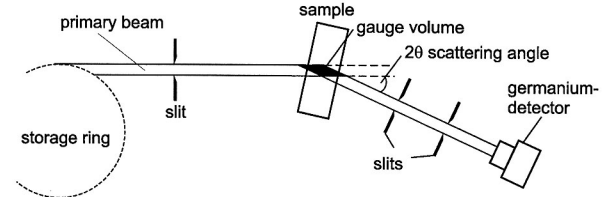

Fig. 1. Schematic illustration of the high-energy synchrotron experiment at the ID 15.

The lattice spacing d^{hkl} can be calculated according to Bragg's law, which can be written as a function of the energy E^{hkl}:

$$d^{hkl} = \frac{hc}{2 \sin \theta} \cdot \frac{1}{E^{hkl}} = \text{const.} \cdot \frac{1}{E^{hkl}} \qquad (1)$$

Here hkl denote the Miller's indices, θ is the Bragg angle, h is Planck's constant and c is the velocity of light. The strain $\varepsilon_{\phi\psi}$ at the sample orientation ϕ, Ψ is evaluated from the measured shift of the lattice spacing:

$$\varepsilon_{\phi\psi}^{hkl} = \frac{d_{\phi\psi}^{hkl}}{d_0} - 1 = \frac{E_0}{E_{\phi\psi}^{hkl}} - 1 \qquad (2)$$

d_0 denotes the lattice parameter of the stress-free material and E_0 is the corresponding energy value. Assuming an uniaxial stress state the stress σ can be calculated from the strain ε^{hkl} using Hooke's law:

$$\sigma = \frac{\varepsilon^{hkl}}{\frac{1}{2} s_2^{hkl} + s_1^{hkl}} \qquad (3)$$

$\frac{1}{2}s_2^{hkl}$ and s_1^{hkl} denote the Diffraction Elastic Constants (DEC) which are specific for each lattice plane. In the case of high energy X-ray diffraction only small scattering angles ($2\theta < 10$ deg) are useful for the registration of spectra, because the atomic scattering factor decreases with $\sin\theta/\lambda$. According to Bragg's equation, a higher energy, that is, a shorter wavelength, corresponds to a lower diffraction angle θ for the same lattice plane. Usually, due to the small scattering angle the measurements are performed in transmission mode (Fig. 1). In this case, the gauge volume element determined by slits in the primary and reflected beam has the shape of a parallelepiped.

3. EXPERIMENTAL PROCEDURE AND DATA EVALUATION

The experiments were carried out with a modified setup on the triple axis diffractometer at the High Energy
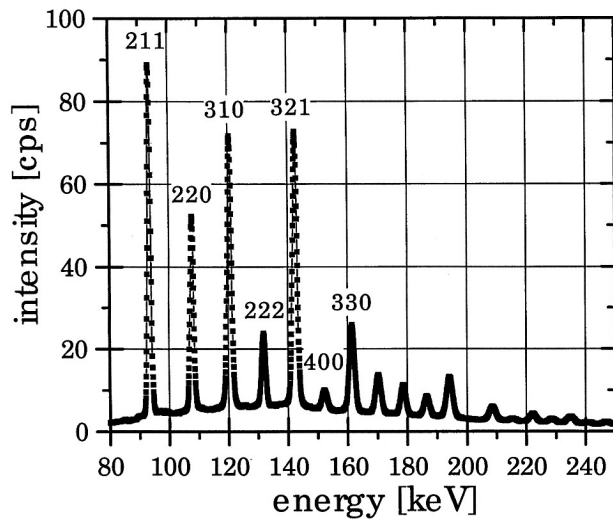
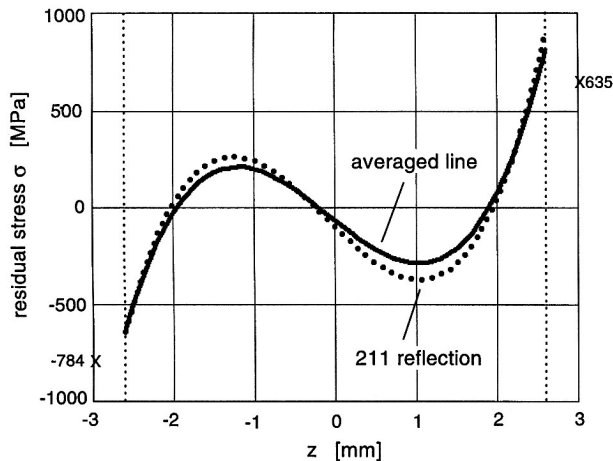**Fig. 2.** Spectrum of the plastic bent steel sheet.

Fig. 3. Residual stress distribution sample in load direction over the sample thickness of the plastic deformed steel sample (buckling line ⊥ measuring plane).

Diffraction Beamline (ID 15A) of the ESRF in Grenoble, France.[13,14] The setup allows investigations in the energy range up to 300 keV. The measurements, except those on a plastic bent steel sheet, were performed at a diffraction angle of $2\theta = 10$ deg. The gauge volume was defined by a slit in the primary beam and two slits in the diffracted beam with an opening width of 80 μm in the diffraction plane. Therefore, the gauge volume is a parallelepiped with the dimensions 1.65 mm perpendicular to the scattering vector and 0.15 mm parallel to it.

3.1. Plastic Bent Steel Sheet

For calibration purposes, measurements were performed at a scattering angle of $2\theta = 6.5$ deg on a steel sheet (German grade: 42CrMo4) with the dimension (width × height × thickness) of $150 \times 40 \times 6$ mm^3, which was plastically deformed in a three-point bending device before the measurements.

Figure 2 shows the intensity distribution and the profile positions with the Miller's indices hkl in the energy diagram, which was registered with a measuring time of 1000 sec. For the evaluation of stress values, the first five reflections were considered.

Apart from proving the reliability of the method and of the obtained data these measurements were performed to check an evaluation method developed for high energy X-ray laboratory measurements in the bulk of material, where the gauge volume is larger than the sample volume.[3] Therefore, in this experiment the extension of the gauge volume perpendicular to the scattering vector was chosen to be 14.2 mm by opening the slits to 0.5 mm. The width at the center is 0.8 mm and the height of the gauge volume is 0.2 mm. The sample translation through the gauge volume was carried out parallel to the reflecting lattice planes from one sharp edge of the parallelepiped to the other one.

As a consequence of the ratio of sample thickness to extension of the gauge volume always integral information over the whole sample thickness is obtained. Furthermore, the center of information defined as the geometrical center of gravity of the intersection of sample volume and gauge volume translates with the sample. Therefore, the strain and stress at each location within the sample can only be determined using a weight function derived from the intensity distribution at several sample positions.[3] Apart from that the sample translation results in a 2θ-shift which has to be corrected by formulas derived from geometrical considerations.[3] In case of the experiments described further on, the above-mentioned corrections with respect to the stress distributions as well as the 2θ-shift can be neglected since the gauge volume is completely within the sample. Figure 3 presents the residual stress distribution $\sigma(z)$ determined by high energy synchrotron diffraction in load direction over the sample thickness of the plastically bent steel sheet. Additionally, the stress values -784 MPa and 635 MPa obtained from conventional X-ray stress analyses performed at the sample surfaces are marked at the ordinate axes. The vertical lines at $z = \pm$ 2.6 mm represent the minimum information depth of 0.4 mm at both surfaces. These z positions were the first
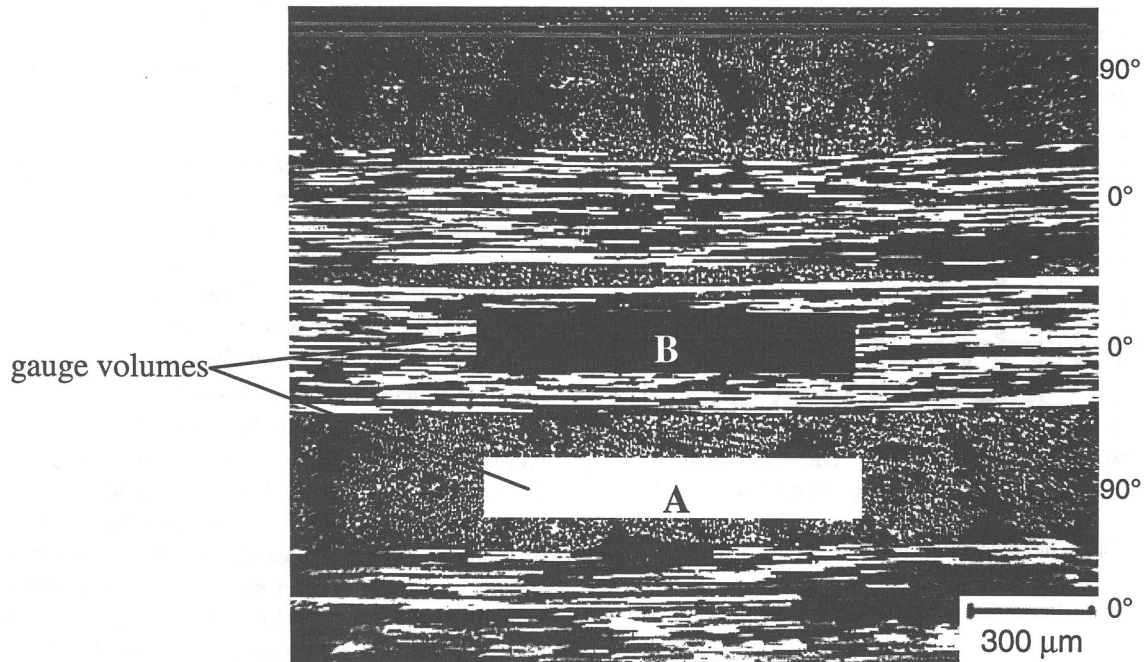
Fig. 4. Arrangement of the layers and position of the gauge volumes A and B in a C/SiC sample.

respectively last location where the reflections could be detected during the sample translation through the gauge volume. This minimum information depth corresponds to a minimum penetration depth of the effective gauge volume of approximately 1.2 mm. The residual stress distribution given by the full line is an average of the stress values obtained from several reflections. For comparison the residual stress distribution determined only using the 211 reflection is shown using a dotted line. The good agreement of the curves proves that the scatter of the high energy synchrotron diffraction data is small. The experimental values are in good agreement with a calculated residual stress distribution.[15] They furtheron correspond to the results of the accompaning high energy X-ray laboratory measurements where the extension of gauge volume was twice as large as in case of the high energy synchrotron diffraction. However, due to the higher local resolution the residual stress distribution obtained by high energy synchrotron diffraction is more pronounced compared to the resolution obtained by the high energy X-ray laboratory measurements.

3.2. Fiber Reinforced Ceramic Composites (CMC)

In fiber-reinforced ceramic composites, residual stresses arise due to the shrinkage of the matrix during the pyrolytical process and also due to the thermal mis-

match between the fibers and the matrix. Here, high energy synchrotron residual stress analysis was performed on a ceramic matrix composite (CMC),.which consists of a SiC matrix reinforced with carbon fibers. The sample was produced by infiltration and pyrolysis of SiC-powder filled polymers (Dornier GmbH, Germany).[16] The structure of the sample is a laminate structure, where each layer of fibers is unidirectional. The layer thickness is approximately 250 µm. The layers are arranged alternately shifted around 90 deg (Fig. 4). The aim of the high energy synchrotron experiments is the determination of the residual stress state in different layers of the SiC matrix, parallel, and perpendicular to the fibers.

The measurements were performed in two positions A and B at the front side of the sample (Fig. 4) and in two directions (0 deg and 90 deg) of the sample. The height of the gauge volume corresponded to the thickness of the layer.

Since SiC exists in two modifications, a cubic, low-temperature modification (β-SiC) and a hexagonal, high-temperature modification (α-SiC) and it also has more than 74 different polytypes, which differ in their stacking modes,[17] first the reflections had to be identified (Fig. 5).

Then the SiC-reflections 6H 110, 3C 220, and 6H 116, 3C 311 (6H means hexagonal with the stacking
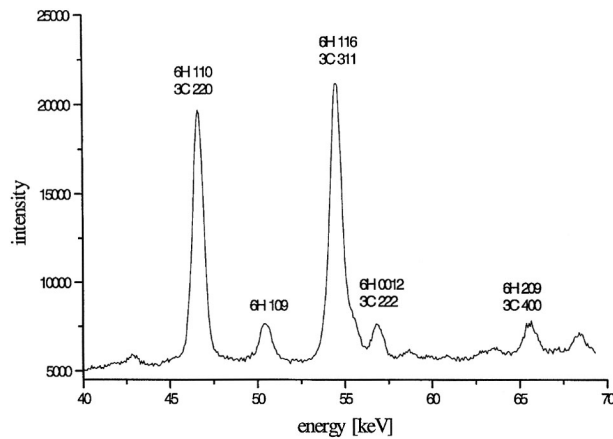
Fig. 5. Part of the spectrum of a C/SiC sample.

order ABCACB; 3C means cubic with the stacking order ABC) were chosen for residual stress evaluation, because these reflections in both directions of measurement have sufficient intensity. From the d-values obtained, the in-plane stresses in the SiC matrix were calculated applying the $\sin^2\Psi$-method.[18] The DEC for the SiC were calculated by the Kröner model using the single crystal constants given in Refs. 19 and 20.

The measurements in gauge volume A (Fig. 4) in both directions of measurement yield the residual stress in the SiC matrix perpendicular to the fibers. The average residual stress for the two combinations of reflections (6H 110 and 3C 220 resp. 6H 116 and 3C 311) is -30 ± 40 MPa. In gauge volume B (Fig. 4), the measurement direction is parallel to the fiber orientation. When the sample is rotated around 90 deg, the measurement direction is perpendicular to the fiber orientation. The height of the gauge volume corresponded to the thickness of the layer. Here, the residual stress in the SiC matrix parallel to the fibers is 230 ± 80 MPa.

3.3. Functional Gradient Material (FGM)

Functional gradient materials (FGM), which differ by composition, phase distribution, porosity, texture as well as related properties such as hardness, density, Young's modulus etc. offer the possibility to optimize their properties in view of the practical use. Due to the difference of the thermal expansion coefficient and the mechanical properties of the constituents residual stresses arise during cooling of a ceramic metal composite from fabrication temperature to room temperature.[21] For analyzing the residual stresses in both phases of a microwave sintered Al_2O_3-Mo sample with a non-

linear composition gradient high energy synchrotron measurements were performed.

The dimensions of the sample were $35 \times 15 \times 10$ mm^2. The measurements were recorded with a counting time of 1000 sec. Figure 6a presents the position and the extension of the gauge volume within the sample. The larger dimension of the gauge volume was chosen to lie perpendicular to the composition gradient and the scattering vector. For residual stress and phase analysis measurements were performed within the composite, additional measurements were carried out within pure Mo and Al_2O_3 in order to determine the stress-free lattice parameter of the phases.

In Fig. 6b, an energy spectrum of a measurement performed within the bulk of the FGM composite is presented. The qualitative phase analysis reveals only Mo and Al_2O_3, the quantitative phase analysis[22] yields a composition of 27 ± 8 vol.% Al_2O_3 and 73 vol.% Mo within the gauge volume.

Assuming a hydrostatic stress state within the gauge volume, the phase specific residual stress (Fig. 7) in the Al_2O_3 and the Mo was calculated using Hooke's law and the DEC calculated from the single crystal elastic constants[23] applying the Kröner model. The stress values reveal that the Al_2O_3 is under compressive and the Mo is under tensile residual stresses, which is a consequence of the stronger contraction of the Al_2O_3 during the cooling caused by its larger thermal expansion coefficient.

In case of Mo, the phase specific residual stress values obtained from the individual peak profiles are in good agreement. Several of the Al_2O_3 peaks, however, are superimposed by the Mo profiles. The evaluation of the remaining Al_2O_3 reflection due to its low intensity results in a comparatively large uncertainty. In order to achieve a better accuracy further measurements with longer counting times and the use of thinner samples is planned in order to be able to evaluate reflections at lower energy levels.

3.4. Metal Ceramic Layer Compound

Investigations were performed in a duplex thermal barrier coating (TBC) system consisting of a plasma sprayed ZrO_2-7 wt.% Y_2O_3 ceramic layer with a thickness of 0.5 mm and a NiCoCrAlY bond layer with a thickness of 0.15 mm, both deposited on a Ni-superalloy In718 substrate with a thickness of 2 mm. The dimensions of the rectangular specimen were $50 \times 10 \times 2.65$ mm^3. In order to analyze the stress state of the bond coat between the ceramic layer and the substrate in dependence of an applied load, a 4-point bending device was
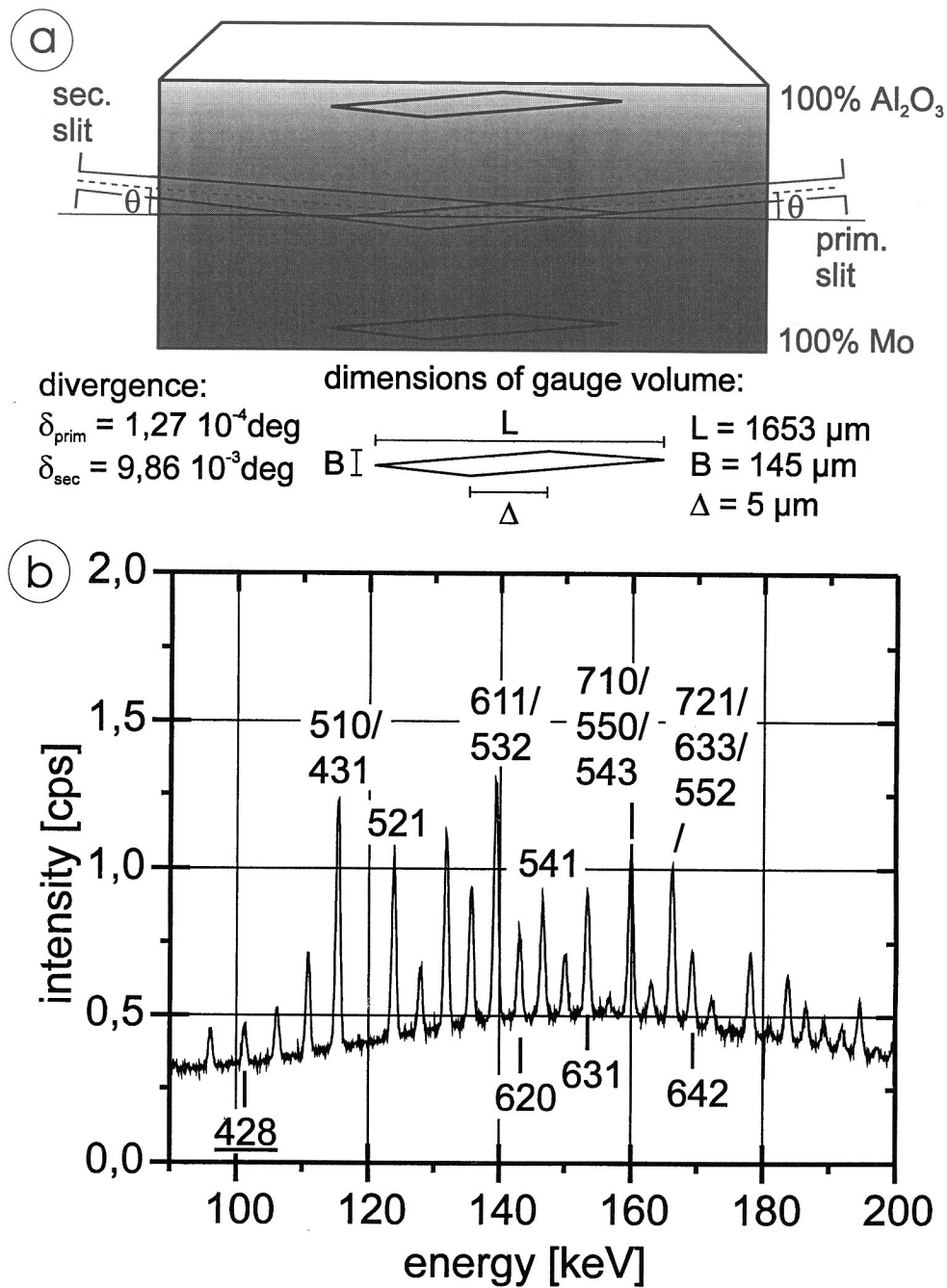
Fig. 6. (a) Gauge volume position in the sample, (b) spectrum of a Al_2O_3-Mo FGM (the Miller's indices of the Al_2O_3-profiles are underlined).

used. The measurements were performed in the transmission mode first without load and then at two different load levels (76 MPa and 114 MPa) using the experimental setup described in Sect. 3.2. In Fig. 8, the scanning of the sample for each external load is shown schematically.

For graphical reasons the gauge volume is shifted vertically in Fig. 8. The 4-point bending device is suggested by the four black circles. The sample has been translated perpendicular to the direction of the external load. Obviously, the diffracted intensity at several sample positions contains information from different layers.
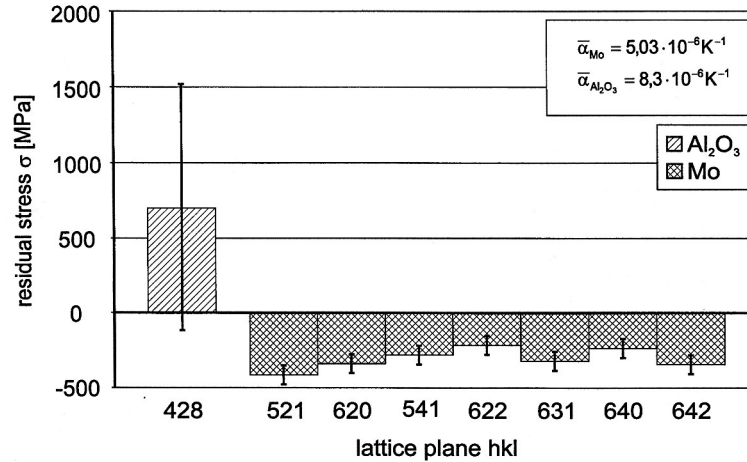
Fig. 7. Phase specific microstresses in a microwave sintered Al_2O_3-Mo FGM.

In Fig. 9 an example for the diffraction pattern is shown for various distances between the center of the gauge volume and the ZrO_2-7 wt.% Y_2O_3 surface defined as zero.

Figure 9 reveals that some reflections only occur at certain distances x from the sample surface. Especially at an energy of 188 keV, a reflection increases in intensity with increasing distance x. It vanishes for distances x larger than the whole thickness of the ceramic and the bond coat layer. Thus, it can be clearly identified as a reflection of the bond coat. This is even more obvious comparing the intensities of the reflections at different distances x (Fig. 10). The reflections at the three different energies clearly refer to the three layers of the sample. Taking into account the diameter of the gauge volume (1.65 mm), it becomes apparent that the x positions of the maximum intensity at the energy 138 keV and 188 keV correspond to the maximum diffracting volume of the ceramic and the bond layer.

A comparison of the energy E_n^{hkl} of the bond coat and the ceramic layer at the two different levels of applied load with the energy E_0^{hkl} obtained from the first scan without load and using an adequate rewritten Eq. (3) allows to determine the changes of the stress state $\Delta\sigma_{En}$ of the ceramic layer and the bond coat. As elastic constants the DEC for ZrO_2 +7 wt.%Y_2O_3: $^1/_2 s_2^{hkl} = 24.1 \times 10^{-6}$ MPa^{-1} and $s_1^{hkl} = -2.4 \times 10^{-6}$ MPa^{-1} as well as for NiCoCrAlY: $^1/_2 s_2^{hkl} = 13.65 \times 10^{-6}$ MPa^{-1} and $s_1^{hkl} = -3.16 \times 10^{-6}$ MPa^{-1} were used.[24] Table I summarizes the stress changes in the bond coat and the ceramic layer, which are due to the external load. For comparison the results of conventional X-ray stress analysis at the surface of the ceramic layer are given. Obviously, for the bond coat, no data could be obtained

with conventional X-ray stress analysis, which is due to its low penetration depth. Further, Table I presents the calculated stress variation in the bond coat according to a multilayer model[25] that was extended to bending loads. The calculated and the stress values determined by high energy synchrotron diffraction for the ceramic layer as well as for the bond coat are in good agreement. Thus, Table I gives evidence for the capability of high energy synchrotron radiation to investigate the stress state in thin interface layers.

3.4. Cold Extruded Samples

In full forward extruded samples (Fig. 11), residual stress and texture gradients arise due to strong plastic deformations, which are inhomogeneously distributed across the sample diameter. Here, the residual stress and the texture gradients were studied in a sample, German steel grade C15, that was full forward extruded with a degree of natural strain of $\varphi = 1.2$. Due to the high intensity and high parallelism of the synchrotron beam the gauge volume was small enough so that several volume elements could be investigated across the sample diameter (Fig. 12). As a consequence of the small gauge volume it further could be assumed that the variation of the residual stress and texture within each of the volume elements is negligible.

The energy spectra obtained in the direction parallel and perpendicular to the axis of the sample (Fig. 13) reveal a $\langle 110 \rangle$ fiber texture that is typical for cold extruded and cold drawn bcc materials.[26] A comparison of the intensity of the 110 type reflections for the different volume elements across the sample diameter furtheron clearly indicates (Fig. 14) that the maximum
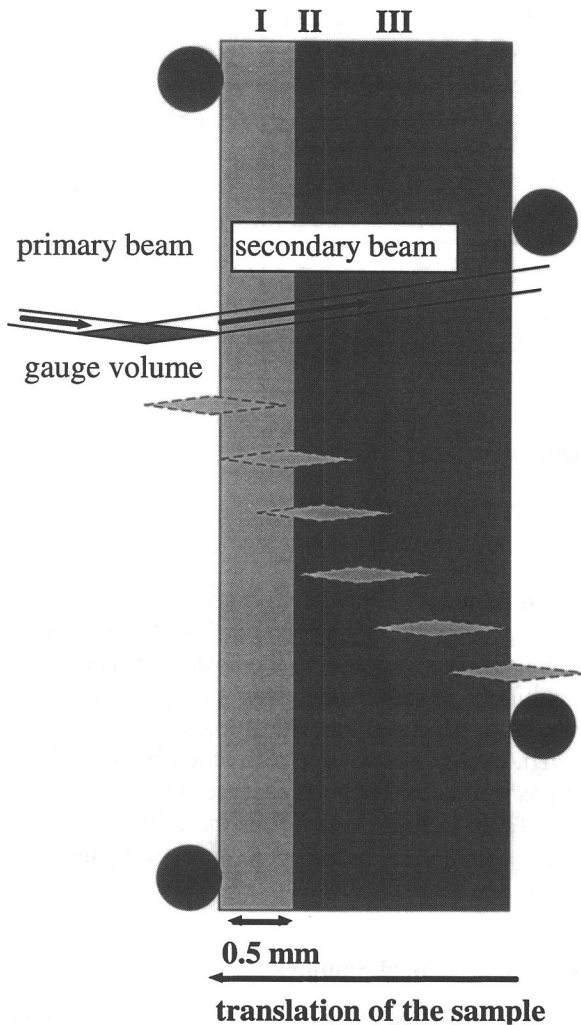
Fig. 8. Scanning of the sample for each external load (schematic). The ceramic layer is marked by I, the bond coat by II and the substrate by III.

Fig. 9. Example for the diffraction pattern for various distances x between the center of the gauge volume and the $ZrO_2 + 7wt\%Y_2O_3$ surface defined as zero.

Fig. 10. Maximum intensity plotted versus distance x between sample surface and center of the gauge volume.

of the texture is in the center of the sample and that the texture is distinctly less pronounced near the sample boundary. Thus, it can be concluded that the plastic deformation is concentrated in the rod kernel, which corresponds to X-ray pole figure and theoretical analyses.[27,28]

From the energy values obtained for the 442, 440, and 541 reflection in radial, hoop, and axial direction of the sample the residual stresses were calculated at the different positions of the gauge volume. The d_0 value necessary for the determination of the three-dimensional residual stress state was calculated as an average of the d values obtained for the different reflections and vol-
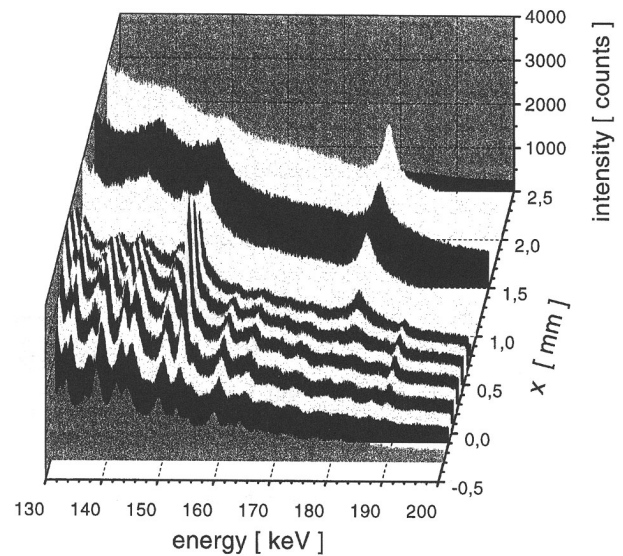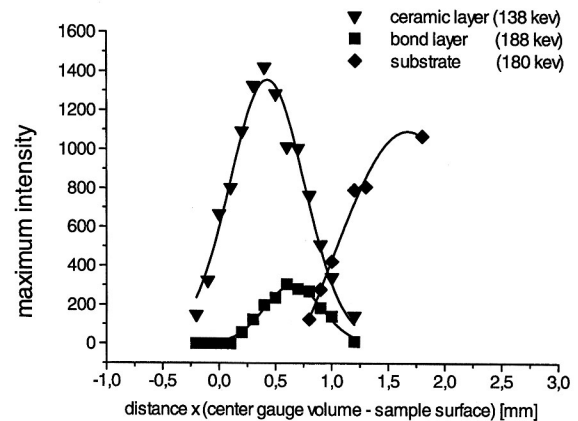
ume elements ("random—walk—method"). Neutron diffraction and synchrotron diffraction in very good agreement reveal that in the inner part of the specimen the residual stresses in radial σ_{rr}, hoop $\sigma_{\phi\phi}$, and axial direction σ_{zz}, are compressive (Fig. 15). These compressive residual stresses are balanced by tensile residual stresses in the outer part of the sample. The quantitative stress values also fulfill within an experimental error margin of ± 80 MPa the mechanical equilibrium condition. At the surface of the sample again compressive stresses in hoop and axial direction were obtained by X-

Table I. Changes of the Stress State in the Thermal Barrier Coating System

external load	material	$\Delta\sigma_{measured}^{synchrotron}$ (MPa)	$\Delta\sigma_{measured}^{X\text{-}ray}$ (MPa)	$\Delta\sigma_{measured}^{external\ load}$ (MPa)
Step I	ZrO_2-7wt.%Y_2O_3-ceramic layer	7 ± 4	5 ± 4	11
	NiCoCrAlY-bond coat	83 ± 18	—	76
Step II	ZrO_2-7wt.%Y_2O_3-ceramic layer	10 ± 4	8 ± 3	16
	NiCoCrAlY-bond coat	118 ± 20	—	114

Fig. 11. Principle of full forward extrusion.

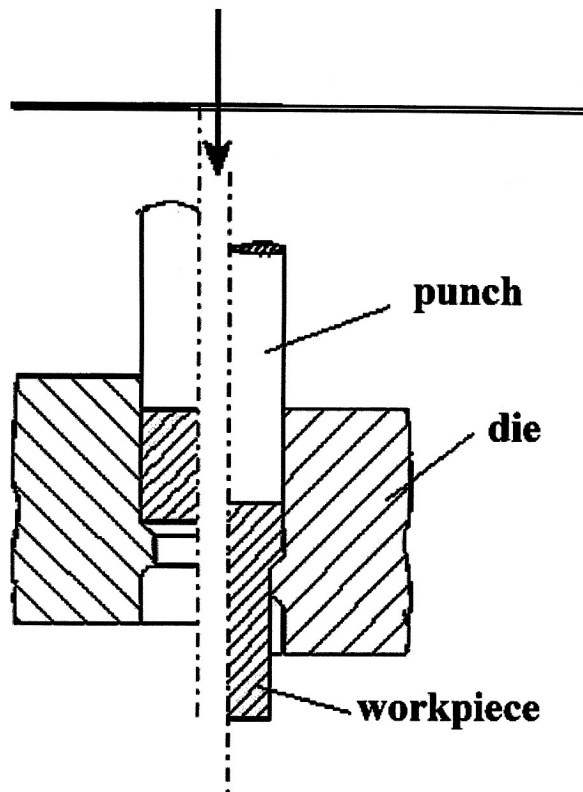Fig. 12. Position of the volume elements.

ray diffraction. This residual stress distribution can be linked to the deformation process during the cold forward extrusion.[27] Due to deformation obstruction at the shoulder of the die, the material flow at the surface is slower and more inhomogeneous than in the inner part of the specimen. Therefore, within the rod kernel the grains are homogeneously stretched whereas at the surface of the sample the grains first are compressed and stretched later, while passing the transient radius of the die. Thus, tensile residual stresses remain in the outer part, while the inner part of the sample is under compressive residual stresses.
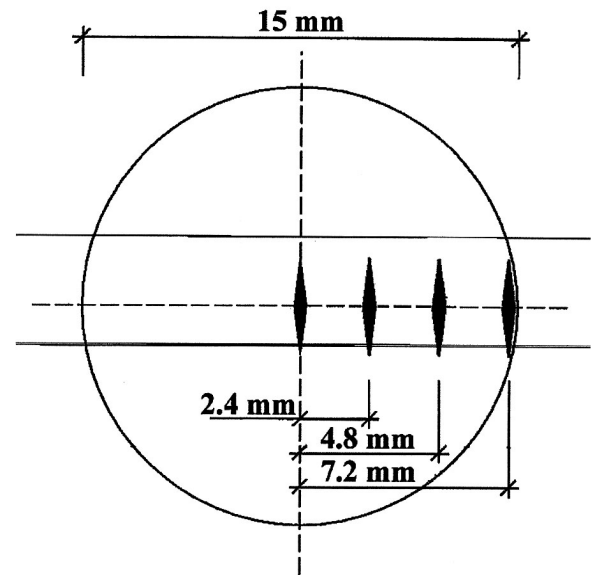
4. CONCLUSIONS

High energy synchrotron diffraction was introduced as a promising new method for the analysis of the triaxial residual stress state. The benefits of the high penetration depth and the superior local resolution, resulting from the high intensity and parallelism of the synchrotron beam as well as advantages resulting from the energy dispersive characteristic of the method, are outlined on the examples of a bent steel bar, composite materials, a ceramic metal layer compound and a cold extruded sample.

The measurements performed with a large gauge volume in the transmission mode on a bent steel bar demonstrate that by using appropriate evaluation methods a stress gradient can be quantitatively determined, although the dimension of the gauge volume is larger than the sample thickness. However, the comparison of these measurements with measurements using a high en-
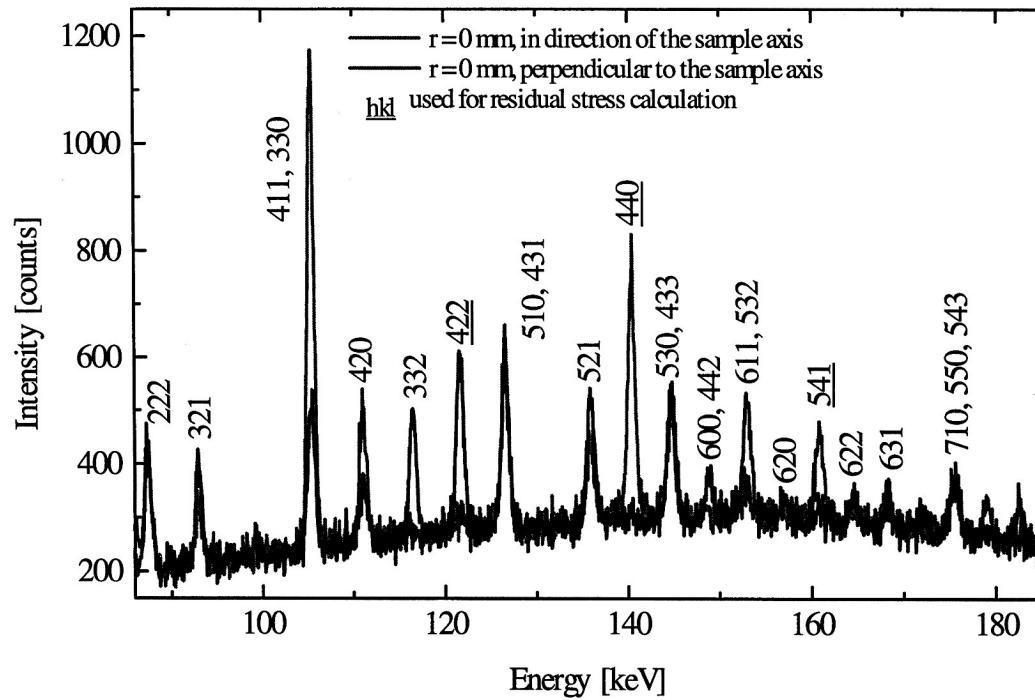
Fig. 13. High-energy synchrotron spectra parallel and perpendicular to the sample resp. fiber axis.
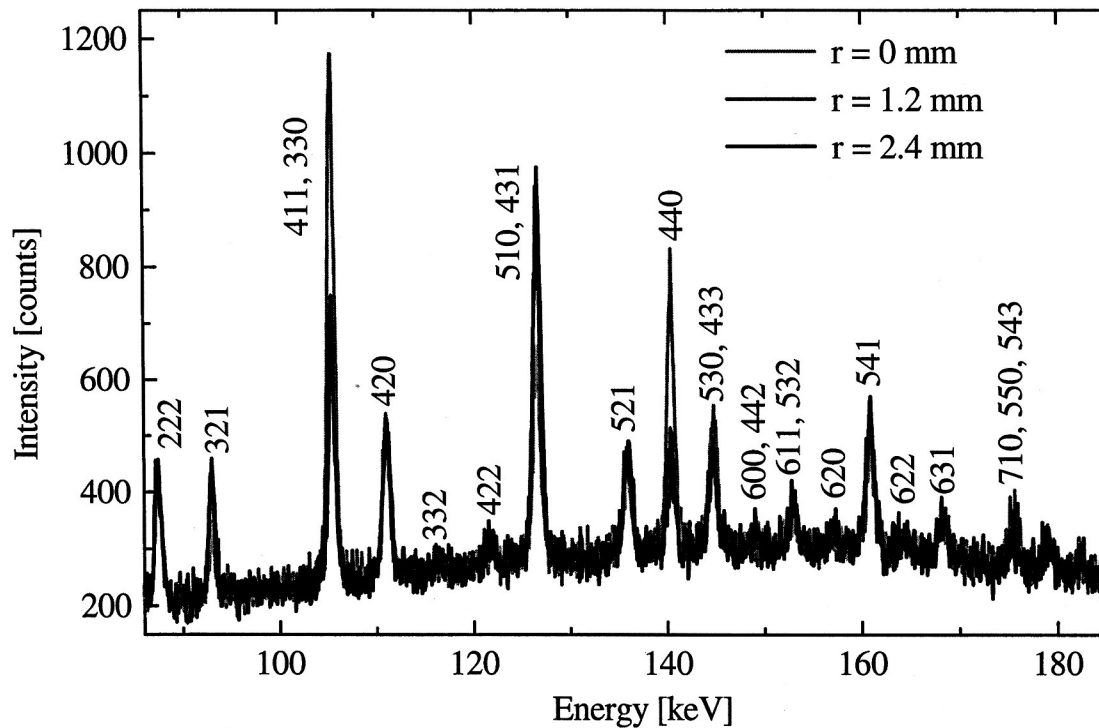

Fig. 14. High-energy synchrotron spectra in direction of the sample axis at different positions across the sample diameter.
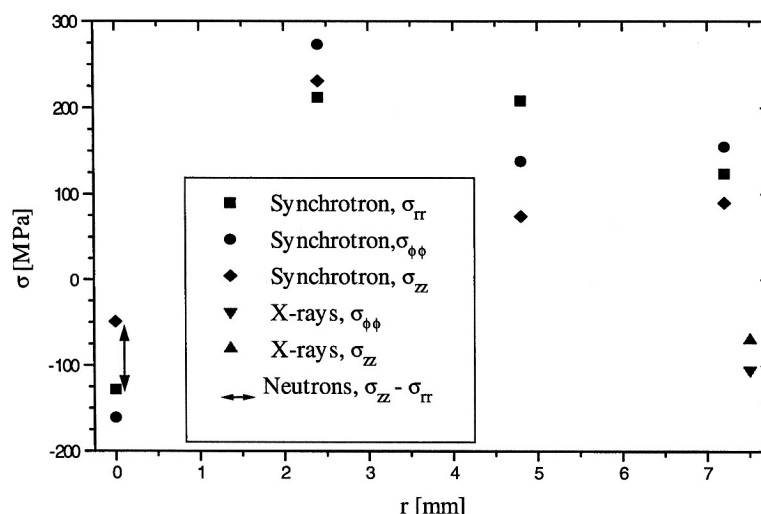
Fig. 15. Residual stress distribution, full forward extruded sample, $\varphi = 1.2$, steel grade C15.

ergy X-ray source in a laboratory reveal the influence of the gauge volume geometry on the resulting values for the stress distribution. It is evident that a further decrease of the gauge volume dimensions, especially perpendicular to the scattering vector will give even more detailed results with respect to the stress distribution. These aspects are important with respect to future residual stress gradient analyses in thin layers.

The results obtained on composite materials reveal that high energy synchrotron diffraction is a suitable method for the evaluation of the triaxial stress state in the bulk of materials. The superior local resolution of high energy synchrotron radiation offers the possibility to analyze the stresses separately in adjacent composite layers and at defined compositions in functional gradient materials, which is not possible using neutrons.

The measurements performed on a ceramic metal layer compound demonstrate for the first time that residual stress values in the interface layer with a thickness of only 100 μm can be determined nondestructively. From the results obtained on cold forward extruded samples it can be concluded that high energy synchrotron diffraction furthermore is very useful for studying residual stress and texture gradients simultaneously.

5. ACKNOWLEDGMENTS

REFERENCES

1. H. Ruppersberg and I. Detemple, *Mater. Sci. Eng.* **A161**: 41–44 (1993).
2. H. Ruppersberg, *Adv. X-Ray Anal.* **35**: 481–487 (1992).
3. G. Brusch and W. Reimers, Proceedings of the ICRS 5, Linköping, Sweden, 1997, pp. 557–562.
4. M. Hutchings, *Neutron News* **3**: 14–19 (1992).
5. L. Pintschovius, in *Measurement of Residual and Applied Stress Using Neutron Diffraction*, M. Hutchings and A. Krawitz, eds. (Kluwer Academic Publisher Dordrecht, Boston, London, 1989), pp. 115–128.
6. C. J. Bechtoldt, R. C. Placious, W. J. Boettinger, and M. Kuriyama, *Adv. X-Ray Anal.* **25**: 330–338 (1981).
7. R. D. Black, C. J. Bechtoldt, R. C. Placious, and M. Kuriyama, *J. Nondestr. Eval.* **5**(1): 21–25 (1985).
8. J. Neuefeind and H. F. Poulsen, *Phys. Scripta* **T57**: 112–116 (1995).
9. H. F. Poulsen, S. Garbe, T. Lorentzen, D. J. Jensen, F. W. Poulsen, N. H. Andersen, T. Frello, R. Feidenhans, and H. Graafsma, preprint (submitted to *J. Synchr. Radiat.*).
10. M. R. Daymond and P. J. Withers, *Scripta Mater.* **35**(10): 1229–1234 (1996).
11. P. J. Webster, X. D. Wang, and G. Mills, *Mater. Sci. Forum* **228–321**: 227–232 (1996).
12. C. G. Windsor, in *Measurement of Residual and Applied Stress Using Neutron Diffraction*, M. Hutchings and A. Krawitz, eds. (Kluwer Academic Publisher Dordrecht, Boston, London, 1989), pp. 285–296.
13. T. Tschentscher and P. Suortti, *J. Synchr. Radiat.* (submitted).
14. P. Suortti and T. Tschentscher, *Rev. Sci. Instr.* **66**(2): 1798–1801 (1995).
15. J. Chakrabarty, *Theory of Plasticity* (McGraw-Hill Book Company, New York, 1987), p. 129.
16. R. Ostertag and T. Haug, in *Advanced Structural Inorganic Composites*, P. Vincenzini, ed. (Elsevier Science Publishers, London, New York, 1991), pp. 469–477.
17. Y. M. Chiang, D. P. Birnie, and W. D. Kingery, *Physical Ceramics-Principles for Ceramic Science and Engineering* (John Wiley & Sons, New York, 1997), pp. 26–33.
18. P. Müller and E. Macherauch, *Z. Angew. Phy.* **13**: 305–312 (1961).
19. G. Arlt and G. R. Schodder, *J. Acoust. Soc. Am.* **37**: 384 (1965).

20. R. M. Martin, *Phys. Rev. B* **6**: 4546 (1972).
21. B. H. Rabin, R. L. Williamson, and S. Suresh, *MRS Bull.* **20**(1): 37–39 (1995).
22. G. Faninger and U. Hartmann, *Härterei Technische Mitteilungen* **27**: 233–244 (1972).
23. Landolt-Börnstein, *Numerical Data and Functional Relationships in Science and Technology, New Series Group III*, Vol. 11, K. Hellwege, ed. (Springer Verlag, Berlin, Heidelberg, New York, 1979), p. 50.
24. U. Baron, T. Cosack, R. Elsing, P. Izquierdo, W. Reimers, G. Schäfer, T. Schmackers, C. Schwaminger, and M. Wildau, Abschlußbericht des BMBF-Projektes: Charakterisierung des Spannungs-Dehnungsverhaltens in Metall-keramischen Schichtverbunden, Fördernummer: 03M 2114 B.
25. O. T. Iancu and D. Munz, *J. Am. Ceram. Soc.* **73**: 1144–1149 (1990).
26. G. Wassermann and J. Grewen, *Texturen metallischer Werkstoffe* (Springer Verlag, Berlin, 1962).
27. A. E. Tekkaya, Ermittlung von Eigenspannungen in der Kaltmasssivumformung, Thesis, Universität Stuttgart (1986).
28. A. Pyzalla and W. Reimers, in *Competitive Advantages by Near-Net-Shape Manufacturing*, H.-D. Kunze, ed. (DGM—Informationsgesellschaft Verlag, Oberursel, 1997), pp. 175–180.